Int J Mech Mater Des (2018) 14:263–275
https://doi.org/10.1007/s10999-017-9368-3

# The role of thermal residual stress on the yielding behavior of carbon nanotube–aluminum nanocomposites

**Mohammad Kazem Hassanzadeh-Aghdam · Mohammad Javad Mahmoodi · Mohammad Reza Kazempour**

Received: 29 November 2016 / Accepted: 28 March 2017 / Published online: 4 April 2017


**Abstract** The initial yield envelopes of aluminum (Al) nanocomposites reinforced with carbon nanotubes (CNTs) subjected to biaxial loading are predicted in the presence of thermal residual stress (TRS) arising from the manufacturing process. Micromechanical model based on the unit cell method is presented to generate the yielding surfaces. The formation of the interphase caused by the interfacial reaction between the CNT and Al matrix is taken into account in the analysis. The effects of several important parameters, i.e. the change of temperature, CNT volume fraction, interphase thickness and Al material properties on the yielding onset of the CNT/Al nanocomposite are explored extensively. The results clearly reveal that the initial yield surfaces of nanocomposite are dependent on the TRS. Also, the interphase has a significant influence on the yielding behavior of Al nanocomposite in the presence of TRS. The results demonstrate that the size of initial yield surfaces become minimum with considering the coupled effects of TRS and interphase. With increasing the temperature variation, interphase thickness, elastic modulus and coefficient of thermal expansion of Al matrix, the size of initial yield surfaces reduces. The present study is consequential for understanding the key role of TRS on the initial damage of CNT/Al nanocomposites.

**Keywords** Carbon nanotubes · Metal-matrix nanocomposites · Yielding behavior · Residual stress · Interphase

## 1 Introduction

Carbon nanotubes (CNTs) possess exceptional combination of mechanical, thermal and electrical properties with high aspect ratio and low density (Pan et al. 2013; Shindo et al. 2014; Aydogdu and Arda 2016; Xu et al. 2012; Cai et al. 2010; Liu and Chen 2003; Joshi et al. 2012). The elastic modulus of CNTs was estimated to be as high as 1 TPa (Fisher et al. 2002). Also, it has been reported that the CNTs have a tensile strength of about 150 GPa (Demczyk et al. 2002). Furthermore, according to the previous studies, the range of elastic deformation and fracture strain of CNTs are exceptionally high (Yakobson et al. 1996; Belytschko et al. 2002).

Because of their high ductility, high strength/weight ratio (specific strength) and resistance to corrosion, aluminum (Al) and its alloys are extensively used as the most important metal matrix materials in composite structures in the various

M. K. Hassanzadeh-Aghdam · M. J. Mahmoodi (✉)
Faculty of Mechanical and Energy Engineering, Shahid Beheshti University, P.O.B. 167651719, Tehran, Iran
e-mail: mj_mahmoudi@sbu.ac.ir

M. K. Hassanzadeh-Aghdam · M. R. Kazempour
Department of Mechanical Engineering, Siyahkal Center, Islamic Azad University, Siyahkal, Iran

industries, especially in aerospace, electronic packaging, renewable energy and automobiles (Starke and Staley 1996; Altenpohl 1998; Esawi et al. 2010; Sharma and Sharma 2016). However, demands on the Al-based structural materials for a better performance under more severe loads and environmental conditions are increasing. One of the ways to enhance the mechanical properties of Al composites is the addition of second phase such as CNTs, due to their excellent properties, into the Al matrix. The experimental reports indicated that the incorporation of CNTs into the Al matrix results in the increase in mechanical properties of Al nanocomposites (Esawi et al. 2010; Sharma and Sharma 2016; Liu et al. 2014; Bakshi et al. 2009; Park et al. 2015; Ci et al. 2006). Furthermore, adding CNTs into the Al matrix leads to a reduction in the value of coefficient of thermal expansion (CTE) of Al nanocomposites (Sharma and Sharma 2016).

Generally, the mechanical properties of Al nanocomposites rely on the dispersion, geometry and volume fraction of the CNTs. Furthermore, the formation of aluminum carbide ($Al_4C_3$) as interphase between Al matrix and CNT has been confirmed by experimental observations (Bakshi et al. 2009; Park et al. 2015; Ci et al. 2006; He et al. 2009; Bakshi and Agarwal 2011; Zhu et al. 2016) which can play an important role in the mechanical properties of these nanocomposites. This interphase is formed due to the chemical interaction between the Al matrix and the CNT. The applied load is transferred to the high strength CNTs through the interfacial layer. It is noted that a strong interface would make the nanocomposite very strong, whereas a weak interface would lead to lower strength. It was reported that $Al_4C_3$ layer could improve the Al-CNT bonding and hinder CNT pull-out (Esawi et al. 2010; Park et al. 2015; Ci et al. 2006; He et al. 2009). Consequently, the improvement in mechanical properties of CNT-reinforced Al nanocomposites can be attributed to the strong interface layer (Park et al. 2015; Ci et al. 2006; He et al. 2009; Bakshi and Agarwal 2011). In this case, a comprehensive study has been accomplished by Bakshi and Agarwal (2011) to show the key role of $Al_4C_3$ layer on the mechanical behavior of Al nanocomposites. By comparing the tensile data of CNT/Mg nanocomposites, CNT/Cu nanocomposites and CNT/Al nanocomposites, they revealed that the improvement in mechanical properties is not effective when there is no chemical interaction between metal matrix and CNT (Bakshi and Agarwal 2011).

There have been many attempts to evaluate the mechanical properties of the CNT-reinforced Al nanocomposites by experimental methods (Esawi et al. 2010; Sharma and Sharma 2016; Liu et al. 2014; Bakshi et al. 2009; Park et al. 2015; Ci et al. 2006; He et al. 2009; Bakshi and Agarwal 2011; Zhu et al. 2016). For example, Esawi et al. (2010) conducted some tensile tests to investigate the effect of CNT content on the mechanical properties of Al nanocomposites. The experimental observations demonstrated improvements of up to 50% in tensile strength and 23% in elastic modulus for Al nanocomposite containing 5 wt% CNTs in comparison with pure Al. Sharma and Sharma (2016) reported the elastic and thermoelastic properties of Al nanocomposites reinforced with CNTs. The experimental results indicated that with introducing 5 wt%CNTs, the elastic modulus of the nanocomposite enhances by 20% compared with that of pure Al, whereas the CTE of the nanocomposite decreases to 70%. Also, the influences of CNT content and temperature on the thermo-mechanical properties of Al nanocomposites were examined (Sharma and Sharma 2016). Also, the tensile properties of Al nanocomposites with different CNT volume fractions were evaluated by Liu et al. (2014). The yield stress and ultimate strength of the Al nanocomposites containing 1.5 vol% CNTs increased by about 41 and 25%, respectively, compared with those of the pure Al matrix. By conducting several tensile tests, Park et al. (2015) exhibited that the yield stress and tensile strength of Al nanocomposites improved by 60 and 23%, respectively, with adding 0.2 wt% CNTs. The experimental observations of He et al. (2009) also clearly showed that both tensile strength and elastic modulus Al nanocomposites rise with increasing CNT weight fraction from 0 up to 5%. However, since there are struggles with CNTs dispersion in the Al matrix and production costs (Park et al. 2015; He et al. 2009), synthesis and test of CNT/Al nanocomposites is not economical. For this reason, simulation methods are proper techniques to predict the overall behavior of these nanocomposites. Moreover, from the viewpoint of experimental, it is very difficult to achieve comprehensive knowledge on the effect of the interphase region on the final CNT/Al nanocomposite effective properties.

One of the effective tools for analyzing the mechanical behavior of CNT-reinforced polymer nanocomposites (Alian et al. 2015a; Wernik et al. 2012; Wernik and Meguid 2011; Tsai et al. 2010; Han and Elliott 2007) and CNT-reinforced metal matrix nanocomposites (Meguid and Al Jahwari 2014; Choi et al. 2016; Song and Zha 2010; Silvestre et al. 2014; Junfeng et al. 2017) is the molecular dynamics (MD) simulations. For instance, in the case of metal matrix nanocomposites, Meguid and Al Jahwari (2014) developed the MD simulations of pullout tests to examine the influences of the different parameters on the interfacial shear strength (ISS) of CNT-reinforced metal matrix nanocomposites. They studied the effects of the cell size, cell geometry, and the potential functions adopted in the MD simulations. The results indicated that the MD cell length has an unimportant effect on the pullout force. Also, Choi et al. (2016) probed the mechanical response of Al nanocomposites containing different types of CNTs subjected to a tensile loading condition using MD simulations. Their outcomes demonstrated that both the elastic modulus and yield stress of CNT-reinforced Al nanocomposites significantly rise, even with a small amount of CNT (Choi et al. 2016). By employing the MD simulations, Song and Zha (2010) studied the influence of Ni coating on the CNT surfaces in terms of the mechanical strengthening of CNT/Al nanocomposites. According to the obtained results, the elastic modulus of the Ni-coated CNT-reinforced Al nanocomposite was noticeably larger than that of the uncoated CNT-reinforced Al nanocomposite (Song and Zha 2010). Later, Silvestre et al. (2014) analyzed the characterization of the mechanical behavior of the Al nanocomposites containing CNTs under compression utilizing the MD simulations. In comparison with pure Al, the increase in elastic modulus due to the addition of CNTs ranged from 50 to 100% (Silvestre et al. 2014). Recently, Junfeng et al. (2017) applied the MD simulations to characterize the strengthening and the deformation mechanisms in the case of CNT-reinforced Al nanocomposites. The effects of both length and diameter of CNTs on the tensile properties of the Al nanocomposites were explored too (Junfeng et al. 2017).

Additionally, the micromechanics approaches have been successfully applied to predict the mechanical behavior of CNT-reinforced polymer nanocomposites (Seidel and Lagoudas 2006; Ray 2010; Ngabonziza et al. 2011; Alian et al. 2015b; Pantano and Cappello 2008) and CNT-reinforced metal matrix nanocomposites (Kashyap et al. 2011; Nouri et al. 2012; Alfonso et al. 2015; Ansari et al. 2016). For instance, in the case of Al-based metal matrix nanocomposites, Kashyap et al. (2011) used the shear lag model to estimate the stiffness of Al nanocomposite with different CNT volume fractions. Also, Nouri et al. (2012) evaluated the stiffness of CNT/Al nanocomposites by employing finite element method (FEM). Alfonso et al. (2015) analyzed the effect of interphase between the CNT and Al matrix on the stiffness of CNT/Al nanocomposites using FEM. The influences of interphase thickness and CNT volume fraction on the elastic behavior of Al nanocomposite were investigated. Moreover, Ansari et al. (2016) studied the stiffness and biaxial initial yield surfaces of CNT/Al nanocomposites through the unit cell micromechanical model. They examined the influences of interphase and CNT volume fraction on the mechanical response of Al nanocomposite. The estimated elastic modulus from the unit cell micromechanical model showed good agreement with experimental data. It should be noted that during the fabrication process, due to mismatch between the CTEs of the constituents of the CNT/Al nanocomposites (Park et al. 2015), the thermal residual stresses (TRSs) can be generated. According to the literature survey, the effects of TRS on the yielding behavior of CNT/Al nanocomposites have not yet been clarified.

The main objective of the present work is to investigate the role of TRS on the initial yielding behavior of CNT-reinforced Al nanocomposites. The remainder of this paper is organized as follows. In Sect. 2, the representative volume element (RVE) of the model is described. In Sect. 3, the simplified unit cell (SUC) micromechanical formulations are presented. In Sect. 4, the SUC simulation results are provided. Finally, in Sect. 5, our findings are summarized.

## 2 RVE of the model

In the micromechanics modeling of CNT-reinforced nanocomposites, a RVE is selected to characterize a small repeatable area of the cross-section of the nanocomposite with the same material properties as those of the nanocomposite materials (Zarasvand and

Golestanian 2016; Herasati and Zhang 2014; Pal and Kumar 2016; Kiani 2016; Long et al. 2015; Nafar Dastgerdi et al. 2013). Figure 1 presents the RVE of the micromechanical unit cell model to simulate the CNT/Al nanocomposites. In the selected RVE, the contours of $i$ and $j(i,j=1,2,3)$ stand for the location of the sub-cell along the $x$- and the $y$ directions, respectively. Consequently, each sub-cell is denoted by $ij$. $L_c$ and $L_r$ stand for the lengths of RVE in the $x$ and $y$ directions, respectively. Also, a unit length in the $z$ direction is considered for the RVE. $d$ and $t_i$ represent the diameter of CNT and the thickness of interphase, respectively.

The constituents of the nanocomposite system are the CNT, Al matrix and the interphase region, as displayed in Fig. 1. The CNT is assumed to be as an equivalent solid nano-fiber (Tsai et al. 2010; Kundalwal and Ray 2011; Shazed et al. 2014; Kundalwal and Meguid 2015; Kundalwal and Ray 2012a) and aligned along the $z$ direction. Thus, $z$ and $x$ (or $y$) directions are the longitudinal and transverse directions, respectively. According to the previous experimental studies (Bakshi et al. 2009; Park et al. 2015; Ci et al. 2006; He et al. 2009), the reaction between the CNT and Al matrix causes the formation of $Al_4C_3$ interphase region. Herein, the interphase is considered as the third phase between the CNT and Al matrix, as illustrated in Fig. 1. Both the CNT and interphase are treated as the linear elastic materials. The Al matrix is assumed to be as an elastoplastic material which obeys

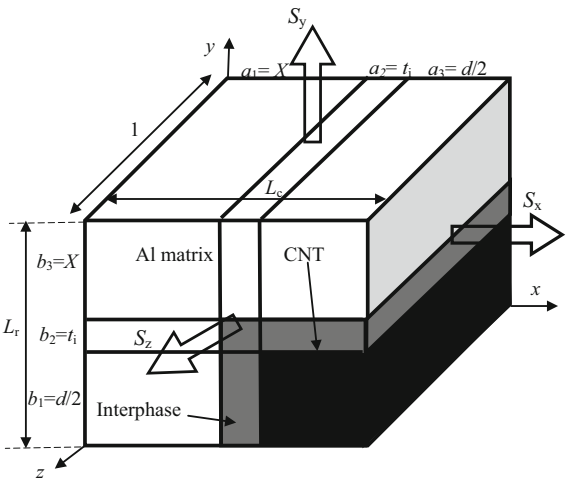


**Fig. 1** RVE of the micromechanical model

the Von-Mises yield criterion. The yielding onset happens as the loading on the CNT/Al nanocomposites is enhanced until the most heavily loaded point within the Al matrix reaches the yield strength ($Y$). Thus, the initial yield strength of the nanocomposite can be expressed as

$$Y=\frac{\sqrt{2}}{2}\sqrt{\left(\sigma_x^{ij}-\sigma_y^{ij}\right)^2+\left(\sigma_x^{ij}-\sigma_z^{ij}\right)^2+\left(\sigma_z^{ij}-\sigma_y^{ij}\right)^2} \tag{1}$$

where $\sigma_x^{ij}$, $\sigma_y^{ij}$ and $\sigma_z^{ij}$ are the normal local stresses in the $x$, $y$ and $z$ directions, respectively, for the sub-cell $ij$ which is occupied by the Al matrix. To generate the initial yield envelopes in longitudinal–transverse and transverse–transverse stress spaces, the RVE is loaded in $z-x$ ($S_z$, $S_x\neq 0$ and $S_y=0$) and $x-y$ ($S_y$, $S_x\neq 0$ and $S_z=0$) directions, respectively. $S_x$, $S_y$ and $S_z$ are the normal global stresses on the RVE, as can be seen in Fig. 1.

## 3 Micromechanical equations

This section presents the SUC micromechanics model to evaluate the behavior of the CNT/Al nanocomposite materials. Assuming the displacement components to be linear, is the basis for deriving the micromechanical equations in the analytical unit cell methods such as method of cell (Kundalwal and Ray 2012b, 2014; Baxter and Robinson 2011) and SUC (Ansari et al. 2016; Ansari and Hassanzadeh-Aghdam 2016a, b, c; Mahmoodi et al. 2010). This assumption results in constant stress and strain state within the sub-cells of the RVE. Moreover, the local shear stresses are not generated inside the sub-cells of the RVE due to the applied normal stresses and vice versa (Ansari et al. 2016; Kundalwal and Ray 2012b, 2014; Baxter and Robinson 2011; Ansari and Hassanzadeh-Aghdam 2016a, b). The following relations can be established by satisfying the equilibrium conditions of the RVE in the normal directions between the applied global stresses and local stresses

$$\begin{cases}\sum_{j=1}^{3} b_j\sigma_x^{1j}=S_xL_r\\ \sum_{i=1}^{3} a_i\sigma_y^{i1}=S_yL_c\\ \sum_{j=1}^{3}\sum_{i=1}^{3} b_ja_i\sigma_z^{ij}=S_zL_rL_c\end{cases} \tag{2}$$

where $a_i$ and $b_j$ are geometric parameters, as displayed in Fig. 1. Imposition of the interfacial traction continuity conditions yields the following relations

$$\sigma_x^{1j} = \sigma_x^{ij} (i > 1), \sigma_y^{i1} = \sigma_y^{ij} (j > 1). \tag{3}$$

The interface between the constituents of the RVE must be considered to be perfect. Thus, the compatibility of the displacements within the RVE can be expressed as (Ansari et al. 2016; Kundalwal and Ray 2012b, 2014; Baxter and Robinson 2011; Ansari and Hassanzadeh-Aghdam 2016a, b)

$$\begin{cases} \sum_{i=1}^{3} a_i \varepsilon_x^{i1} = \sum_{i=1}^{3} a_i \varepsilon_x^{ij} = L_c \bar{\varepsilon}_x (j > 1) \\ \sum_{j=1}^{3} b_j \varepsilon_y^{1j} = \sum_{j=1}^{3} b_j \varepsilon_y^{ij} = L_r \bar{\varepsilon}_y (i > 1) \\ \varepsilon_z^{11} = \varepsilon_z^{ij} = \bar{\varepsilon}_z (i > 1, j > 1) \end{cases} \tag{4}$$

where $\bar{\varepsilon}_x$, $\bar{\varepsilon}_y$ and $\bar{\varepsilon}_z$ are the global strains. Also, $\varepsilon_x^{ij}$, $\varepsilon_y^{ij}$ and $\varepsilon_z^{ij}$ are local strains within the sub-cell $ij$. The constitutive relation for the sub-cell $ij$ is given by

$$\boldsymbol{\varepsilon}^{ij} = \mathbf{S}^{ij} : \boldsymbol{\sigma}^{ij} + \boldsymbol{\alpha}^{ij} \Delta T \tag{5}$$

where $\boldsymbol{\sigma}^{ij}$ and $\boldsymbol{\varepsilon}^{ij}$ are the vectors of the normal stresses and strains of the sub-cell $ij$, respectively. Also, $\mathbf{S}^{ij}$ and $\boldsymbol{\alpha}^{ij}$ are the elastic compliance matrix and the vector of CTE of the sub-cell $ij$, respectively. $\Delta T$ is the temperature change. The following relation can be obtained by the extension of Eq. (5) for each linearly elastic isotropic sub-cell $ij$, as

$$\begin{cases} \varepsilon_x^{ij} = \frac{1}{E^{ij}} \sigma_x^{ij} - \frac{v^{ij}}{E^{ij}} (\sigma_y^{ij} + \sigma_z^{ij}) + \alpha^{ij} \Delta T \\ \varepsilon_y^{ij} = \frac{1}{E^{ij}} \sigma_y^{ij} - \frac{v^{ij}}{E^{ij}} (\sigma_x^{ij} + \sigma_z^{ij}) + \alpha^{ij} \Delta T \\ \varepsilon_z^{ij} = \frac{1}{E^{ij}} \sigma_z^{ij} - \frac{v^{ij}}{E^{ij}} (\sigma_x^{ij} + \sigma_y^{ij}) + \alpha^{ij} \Delta T \end{cases} \tag{6}$$

where $E$ and $v$ are elastic modulus and Poisson's ratio, respectively. Then, substituting Eq. (6) into Eq. (4) in conjunction with Eq. (3) leads to

$$\sum_{i=1}^{3} \left\{ \frac{a_i}{E^{i1}} \sigma_x^{11} - \frac{a_i}{E^{ij}} \sigma_x^{1j} - \frac{a_i}{E^{i1}} v^{i1} \sigma_y^{i1} + \frac{a_i}{E^{ij}} v^{ij} \sigma_y^{ij} - \frac{a_i}{E^{i1}} v^{i1} \sigma_z^{i1} + \frac{a_i}{E^{ij}} v^{ij} \sigma_z^{ij} \right\} = a_i \left( \alpha^{ij} - \alpha^{i1} \right) \Delta T \quad (j > 1)$$

$$\sum_{j=1}^{3} \left\{ -\frac{b_j}{E^{1j}} v^{1j} \sigma_x^{1j} + \frac{b_j}{E^{ij}} v^{ij} \sigma_x^{ij} + \frac{b_j}{E^{1j}} \sigma_y^{11} - \frac{b_j}{E^{ij}} \sigma_y^{i1} - \frac{b_j}{E^{1j}} v^{1j} \sigma_z^{1j} + \frac{b_j}{E^{ij}} v^{ij} \sigma_z^{ij} \right\} = b_j \left( \alpha^{ij} - \alpha^{1j} \right) \Delta T \quad (i > 1)$$

$$\left\{ -\frac{v^{11}}{E^{11}} \sigma_x^{11} + \frac{v^{ij}}{E^{ij}} \sigma_x^{ij} - \frac{v^{11}}{E^{11}} \sigma_y^{11} + \frac{v^{ij}}{E^{ij}} \sigma_y^{i1} + \frac{1}{E^{11}} \sigma_z^{11} - \frac{1}{E^{ij}} \sigma_z^{ij} \right\} = \left( \alpha^{ij} - \alpha^{11} \right) \Delta T \quad (i > 1, j > 1). \tag{7}$$

Considering Eqs. (2), (7), a system of 15 linear equations with the same number of unknowns is generated as

$$[\mathbf{A}]_{15\times15} \{\boldsymbol{\sigma}\}_{15\times1} = \{\mathbf{F}\}_{15\times1} \tag{8}$$

in which $\{\boldsymbol{\sigma}\}$ and $\{\mathbf{F}\}$ are the vectors of stress and the external load, respectively. $[\mathbf{A}]$ is the coefficients matrix. By applying the mechanical loading; i.e. $S_z, S_x \neq 0$, $S_y = 0$ for generating longitudinal–transverse initial yield envelope or $S_y, S_x \neq 0$, $S_z = 0$ for generating transverse–transverse initial yield envelope, as well as thermal loading; i.e. $\Delta T$ for considering the effect of TRS, the values of $\{\mathbf{F}\}$ are specified. Also, $[\mathbf{A}]$ is constructed through the geometrical conditions and material properties of the sub-cells of the RVE. Then, three stress components for all sub-cells can be determined by the solution of Eq. (8). It is noted that the calculated stress components for the Al matrix sub-cell have to satisfy Eq. (1) for generating a yielding point in the stress space.

## 4 Results and discussion

Firstly, a comparison is made between the present study and the work of Ansari et al. (2016). The elastic properties of CNT, Al matrix and interphase are tabulated in Table 1 (Ansari et al. 2016). The values of

**Table 1** Elastic properties of CNT, Al matrix and interphase for comparison purpose (Ansari et al. 2016)

| Material | $E$ (GPa) | $V$ |
|---|---|---|
| CNT | 1000 | 0.3 |
| Al | 73.4 | 0.334 |
| Interphase | 403.7 | 0.334 |

CNT volume fraction (VF), $d$, $t_i$ and $Y$ are equal to 3%, 20, 10 nm and 56 MPa, respectively (Ansari et al. 2016). Figure 2a, b show the results of two works in predicting the initial yield envelopes of nanocomposite in transverse–transverse and longitudinal–transverse stress spaces, respectively. It should be noted that all stresses are normalized with respect to the yield strength of Al matrix. Two sets of results are in excellent agreement as clarified in Fig. 2a, b.

To further validate and guarantee accuracy of the presented model, the results of the presented SUC model are compared with those of FEM (Aghdam et al. 2001) for unidirectional silicon carbide (SiC)-reinforced titanium (Ti) composites. The SiC fiber and Ti matrix are assumed to be strain free at 930 °C and a cool down to room temperature at 23 °C which generates the residual stresses (Aghdam et al. 2001). The material properties of the constituents of the composite are given in Table 2 (Aghdam et al. 2001). Figure 3 shows the initial yield envelope of SiC/Ti composite in transverse–transverse stress space. The SiC volume fraction is 35% (Aghdam et al. 2001). Generally, good agreement exists between the results of the SUC model and FEM (Aghdam et al. 2001), validating the micromechanical model developed in this study.

Now, the role of TRS on the biaxial yielding behavior of CNT/Al nanocomposite is investigated.

**Table 2** Material properties of SiC fiber and Ti matrix (Aghdam et al. 2001)

| Material | $E$ (GPa) | $V$ | $\alpha$ ($10^{-6}$/K) | $Y$ (MPa) |
|---|---|---|---|---|
| SiC | 409 | 0.2 | 4.5 | – |
| Ti | 107 | 0.3 | 10 | 940 |

The material properties of the constituents of nanocomposite are given in Table 3 (Ci et al. 2006; Bakshi and Agarwal 2011; Alfonso et al. 2015). Also, the values of $d$ and $t_i$ are considered as 70 and 15 nm, respectively (Alfonso et al. 2015). The CNT volume fraction is selected as 1% in the analysis. The CNT/Al nanocomposite system is analyzed under a temperature decrease of 450 °C due to the manufacturing process (Ci et al. 2006). Unless otherwise stated, these values are utilized in order to parametric studies. Figure 4a, b depict the coupled effects of interphase region and TRS on the initial yield surfaces of CNT/Al nanocomposite in transverse–transverse and longitudinal–transverse stress spaces, respectively. As a first founding, in the absence of TRS, the effect of interphase on the yielding behavior of nanocomposite can be neglected. However, regardless of the interphase, the size of initial yield surfaces of nanocomposite is highly affected and reduced by the TRS. According to the results in Fig. 4a, b, with considering

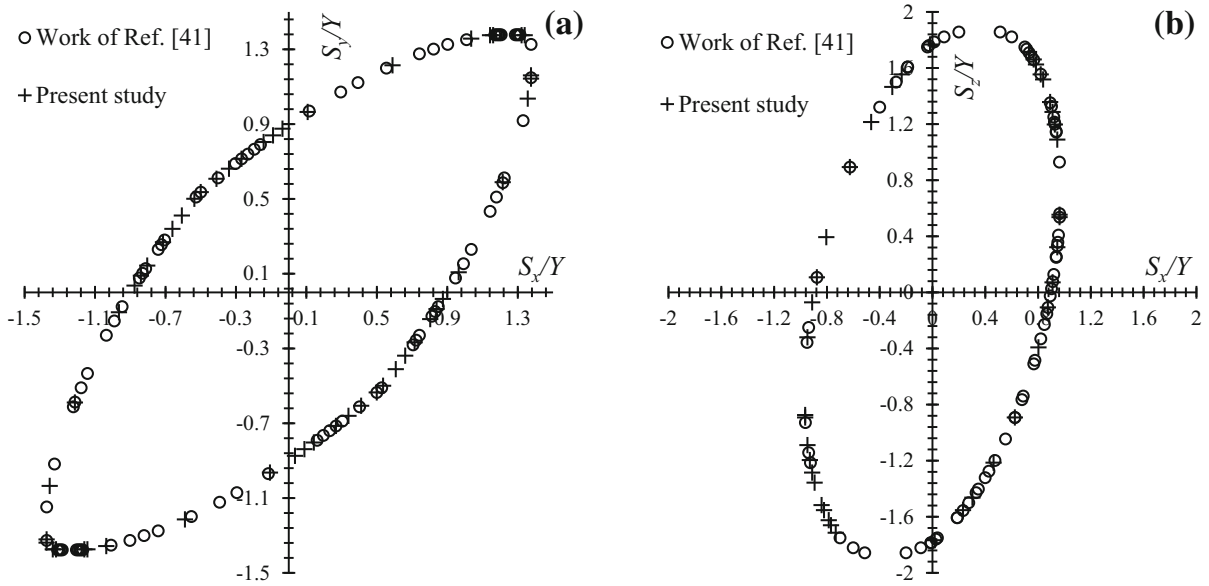


**Fig. 2** Comparison between the results of present study and the work of Ref. (Tsai et al. 2010)

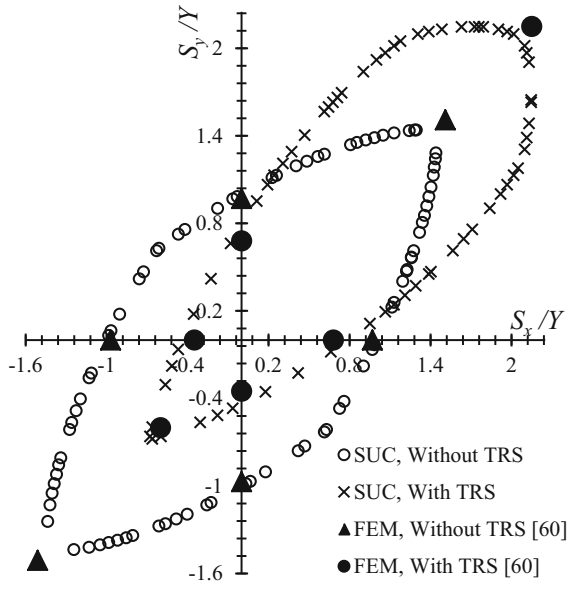


**Fig. 3** Comparison between the results of the presented SUC model and FEM (Aghdam et al. 2001) for SiC/Ti composite

**Table 3** Material properties of the CNT, Al matrix and interphase (Ci et al. 2006; Bakshi and Agarwal 2011; Alfonso et al. 2015)

| Material | $E$ (GPa) | $V$ | $\alpha$ ($10^{-6}$/K) | $Y$ (MPa) |
|---|---|---|---|---|
| CNT | 680 | 0.27 | 1 | – |
| Al | 70 | 0.33 | 23.6 | 262 |
| Interphase ($Al_4C_3$) | 309 | 0.2 | 5 | – |

two factors including TRS and interphase region, the size of initial yield envelopes of the nanocomposite becomes minimum. The results reveal that the TRS shifts the initial yield curve in the transverse plane towards positive transverse stresses, as shown in Fig. 4a. Also, in the presence of TRS, the interphase has the maximum influence on the initial yield envelope in transverse–transverse stress space when $S_x = S_y < 0$. In the presence of TRS, the yield strengths of the CNT/Al nanocomposite under uniaxial transverse tension (i.e. $S_y = 0, S_x > 0$ or $S_x = 0, S_y > 0$) with and without interphase are 150 and 194 MPa, respectively. It is observed from Fig. 4b that the TRS can shift the initial yield surface in the longitudinal plane towards negative longitudinal stress. Also, under uniaxial longitudinal tension (i.e. $S_x = 0, S_z > 0$) and in the presence of the TRS, the yield strength of CNT/Al nanocomposite with interphase is significantly lower than that of the CNT/Al nanocomposite without interphase. However, under uniaxial longitudinal compression (i.e. $S_x = 0, S_z < 0$) and in the presence of the TRS, the effect of interphase on the yield strength is very negligible. With considering the interphase, the yield strengths of the CNT/Al nanocomposite under uniaxial longitudinal tension in the presence and the absence of TRS are 141.5 and 288 MPa, respectively, while yield strengths under uniaxial longitudinal compression in the presence and absence of the TRS are 374.5 and 293.5 MPa, respectively.

Figure 5a, b show the effect of temperature change on the initial yield envelopes of CNT/Al nanocomposite in transverse–transverse and longitudinal–transverse stress spaces, respectively. Three different values, including $\Delta T = -250, -350$ and $-450$ °C are selected for the analysis. As illustrated in Fig. 5a, b, the size of initial yield surfaces significantly decreases with increasing temperature change ($\Delta T$). It is found from Fig. 5a that the value of $\Delta T$ has the maximum effect on the initial yield curve in transverse–transverse stress space when $S_x = S_y < 0$. However, when $S_x = S_y > 0$, the variation of $\Delta T$ very slightly affects the yielding behavior of the nanocomposite in transverse–transverse stress space. Figure 5b shows that the yielding in the nanocomposite under uniaxial longitudinal tension occurs at lower applied loads as the value of $\Delta T$ increases. For instance, the yield strengths of the nanocomposite under uniaxial longitudinal tension are 217.5, 173 and 141.5 MPa for $\Delta T = -250, -350$ and $-450$ °C, respectively. However, the influence of the variation of $\Delta T$ on the initial yield surface in longitudinal–transverse stress space can be neglected when $S_z < 0, S_x = 0$.

Figure 6a, b illustrate the effect of interphase thickness on the initial yield envelopes of CNT/Al nanocomposite in transverse–transverse and longitudinal–transverse stress spaces, respectively. Three different values, including $t_i = 10$, 15 and 20 nm are selected for the analysis. The results reveal that the increase in interphase thickness can decrease the size of the initial yield surfaces of the nanocomposite. Interphase thickness has the maximum effect on the initial yield curve in transverse–transverse stress space when $S_x = S_y < 0$, as can be seen in Fig. 6a. However, when $S_x = S_y > 0$, the initial yield surface in transverse–transverse stress space is independent of the interphase thickness. It is found from Fig. 6b that

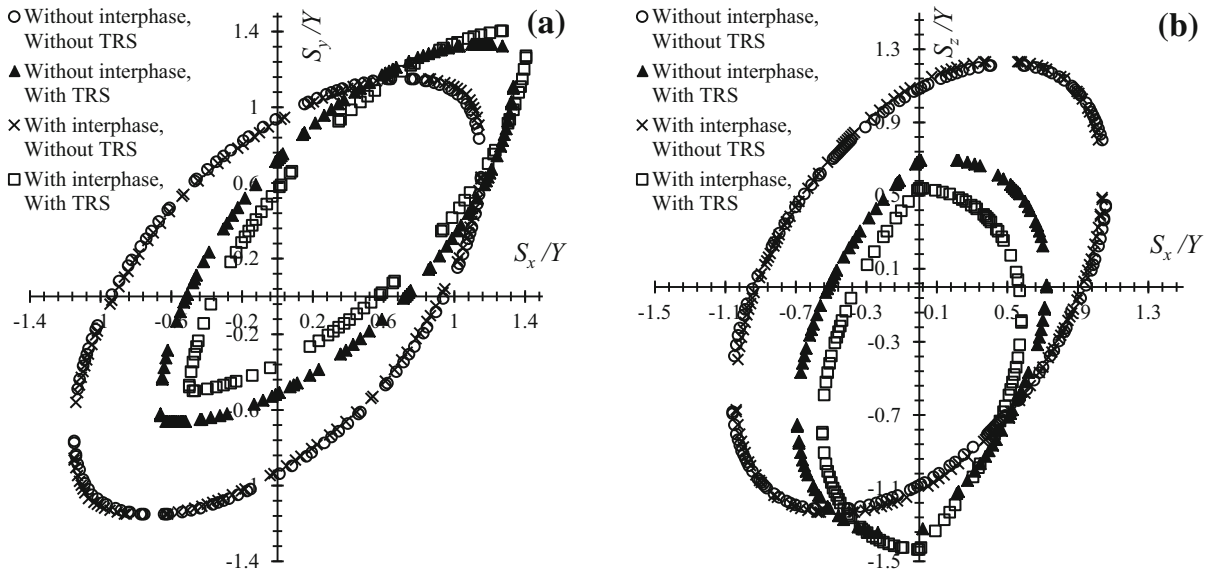


**Fig. 4** Effects of interphase and TRS on the initial yield surfaces in **a** transverse–transverse and **b** longitudinal–transverse stress spaces

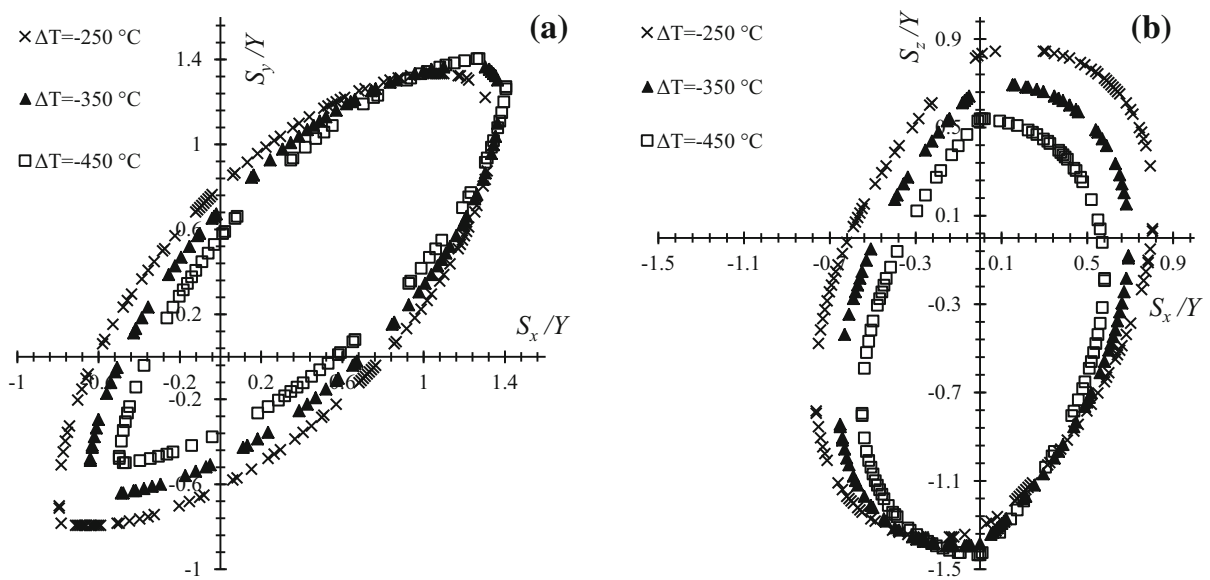


**Fig. 5** Effect of temperature change on the initial yield surfaces in **a** transverse–transverse and **b** longitudinal–transverse stress spaces

yielding of the nanocomposite in uniaxial longitudinal tension happens at lower applied loads with higher interphase thickness. However, in uniaxial longitudinal compression, the yielding behavior of the nanocomposite is not affected by the variation of interphase thickness.

Figure 7a, b display the effect of CNT volume fraction on the initial yield envelopes of CNT/Al nanocomposite in transverse–transverse and longitudinal–transverse stress spaces, respectively. The results in the absence of TRS are also included in Fig. 7a, b. It is found that without TRS, the change in CNT volume fraction can slightly affect the yielding behavior of CNT/Al nanocomposite. However, when the TRS is considered in the micromechanical modeling, the initial yield surfaces of the nanocomposite

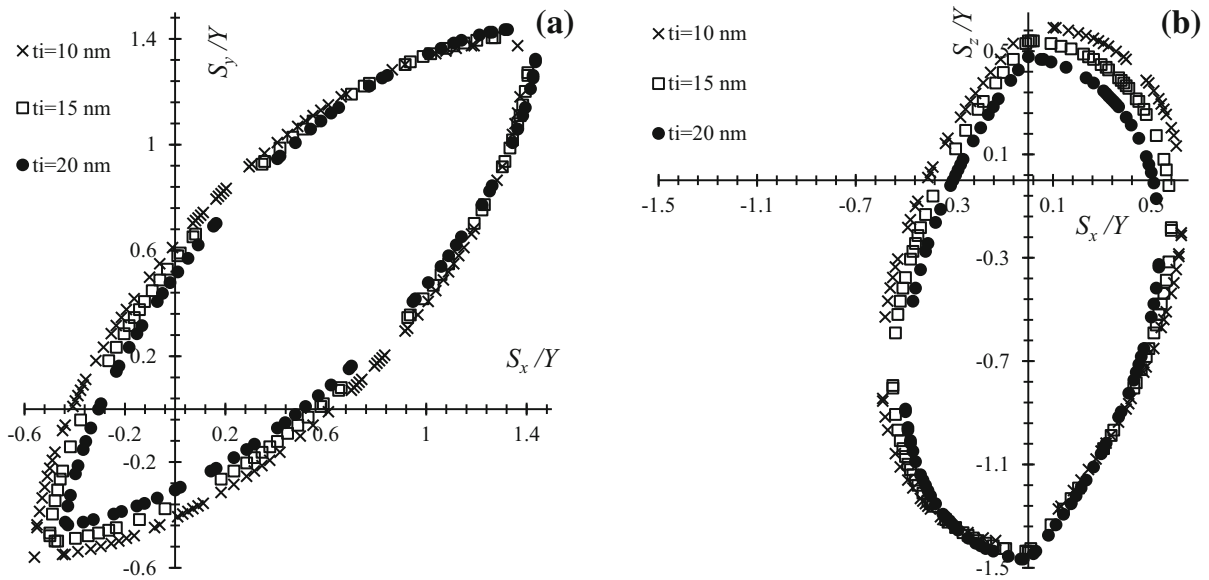


**Fig. 6** Effect of interphase thickness on the initial yield surfaces in **a** transverse–transverse and **b** longitudinal–transverse stress spaces

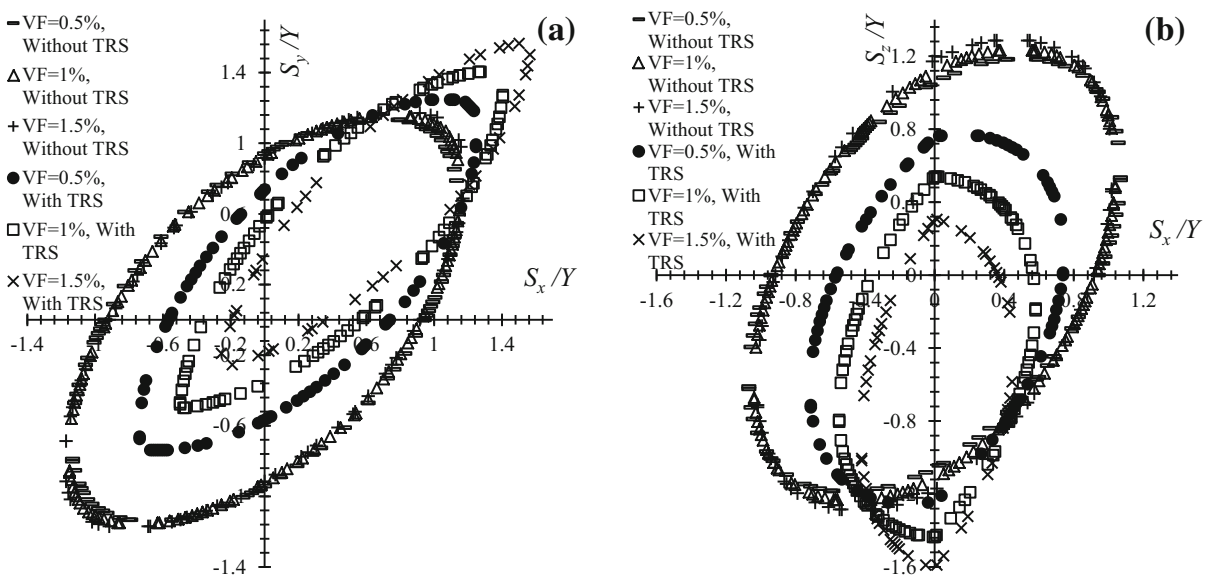


**Fig. 7** Effect of CNT volume fraction on the initial yield surfaces in **a** transverse–transverse and **b** longitudinal–transverse stress spaces

are considerably affected by the change in CNT volume fraction. The results of Fig. 7a demonstrate that the CNT volume fraction has the highest effect on the initial yield surfaces in transverse–transverse stress space when $S_x = S_y$. As presented in Fig. 7b, with increasing the CNT volume fraction and in the presence of TRS, the value of yield strength in uniaxial longitudinal tension decreases while its value in uniaxial longitudinal compression significantly increases.

Figure 8a, b depict the effect of variation in elastic modulus of Al matrix ($E_m$) on the initial yield envelopes of CNT/Al nanocomposite in transverse–transverse and longitudinal–transverse stress spaces, respectively. Three different values, including $E_m = 60$, 70 and 80 GPa are selected for the analysis.

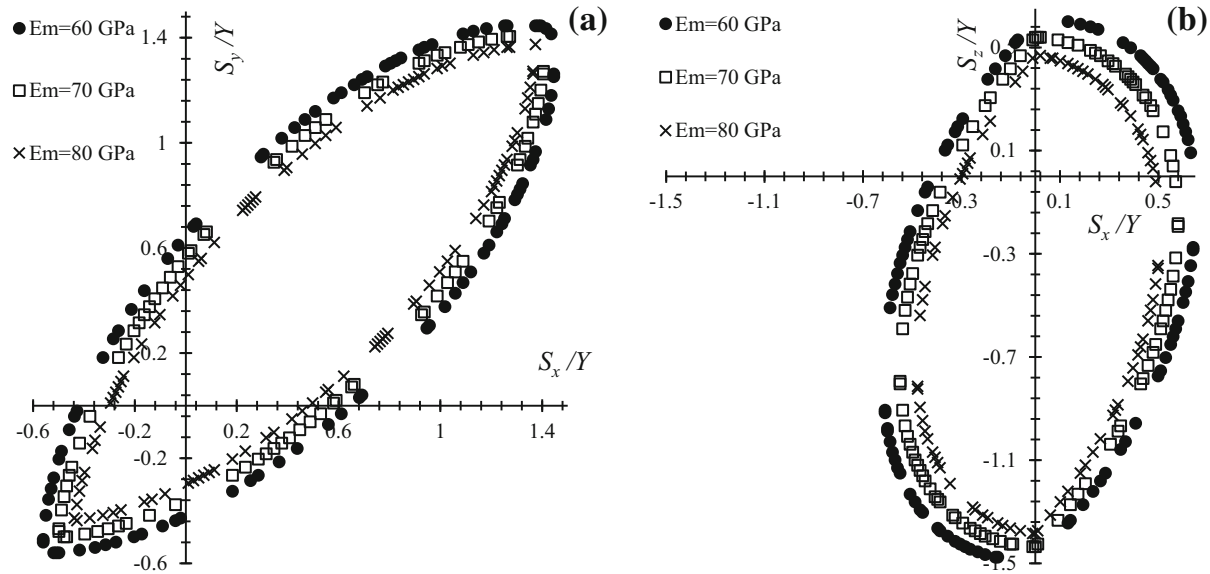


**Fig. 8** Effect of elastic modulus of Al matrix on the initial yield surfaces in **a** transverse–transverse and **b** longitudinal-transverse stress spaces

It should be noted that the effects of interphase and TRS are included in the analysis. The size of initial yield surfaces is affected and reduced with increasing the matrix elastic modulus. As can be seen in Fig. 8a, when $S_y = 0$, $S_x > 0$, the yield strengths of nanocomposite are 131, 150 and 165 MPa for $E_m = 80$, 70 and 60 GPa, respectively. It is found from Fig. 8b, when $S_x = 0$, $S_z > 0$, the yield strengths of nanocomposite are 160, 141.5 and 120.5 MPa for $E_m = 80$, 70 and 60 GPa, respectively.

Figure 9a, b exhibit the effect of yield strength of Al matrix on the initial yield envelopes of CNT/Al nanocomposite in transverse–transverse and longitudinal–transverse stress spaces, respectively. Three different values, including $Y = 212$, 262 and 312 MPa are selected for the analysis. The results are extracted in the presence and the absence of the TRS, as illustrated in Fig. 9a, b. It should be noted that the interphase region is considered in the modeling of CNT/Al nanocomposite. In the absence of TRS, the change of yield strength of Al matrix does not affect the normalized initial yield surfaces of nanocomposite. However, it is identified that the normalized initial yield surfaces to be noticeably insensitive to the change of matrix yield strength in the presence of TRS. The results in Fig. 9a, b reveal that in the presence of TRS, the size of normalized initial yield surfaces of nanocomposite decreases with decreasing the yield strength of Al matrix. As shown in Fig. 9a in the presence of TRS, the change of $Y$ has the highest and lowest effect on the initial yield curves in transverse–transverse stress space when $S_x = -S_y < 0$ and $S_x = S_y > 0$, respectively. Also, it is observed from Fig. 9b that in the presence of TRS, the yield strength of nanocomposite in uniaxial longitudinal tension (i.e. $S_z > 0$, $S_x = 0$) is significantly affected by the change of the value of $Y$. However, the effect of $Y$ on the yield strength of nanocomposite in uniaxial longitudinal compression (i.e. $S_z < 0$, $S_x = 0$) can be ignored.

Figure 10a, b illustrate the effect of CTE of Al matrix ($\alpha_m$) on the initial yield envelopes of CNT/Al nanocomposite in transverse–transverse and longitudinal–transverse stress spaces, respectively. Three different values, including $\alpha_m = 17.6 \times 10^{-6}$, $20.6 \times 10^{-6}$ and $23.6 \times 10^{-6}$ 1/K are selected for the analysis. As displayed in Fig. 10a, b, the size of initial yield surfaces decreases with increasing the value of $\alpha_m$. Figure 10a shows that the change of $\alpha_m$ has the highest and lowest effect on the initial yield surfaces in transverse–transverse stress space when $S_x = S_y < 0$ and $S_x = S_y > 0$, respectively. The change in the value of $\alpha_m$ negligibly affects the yield strength in uniaxial longitudinal compression, as can be seen in Fig. 10b. However, the yield strength of

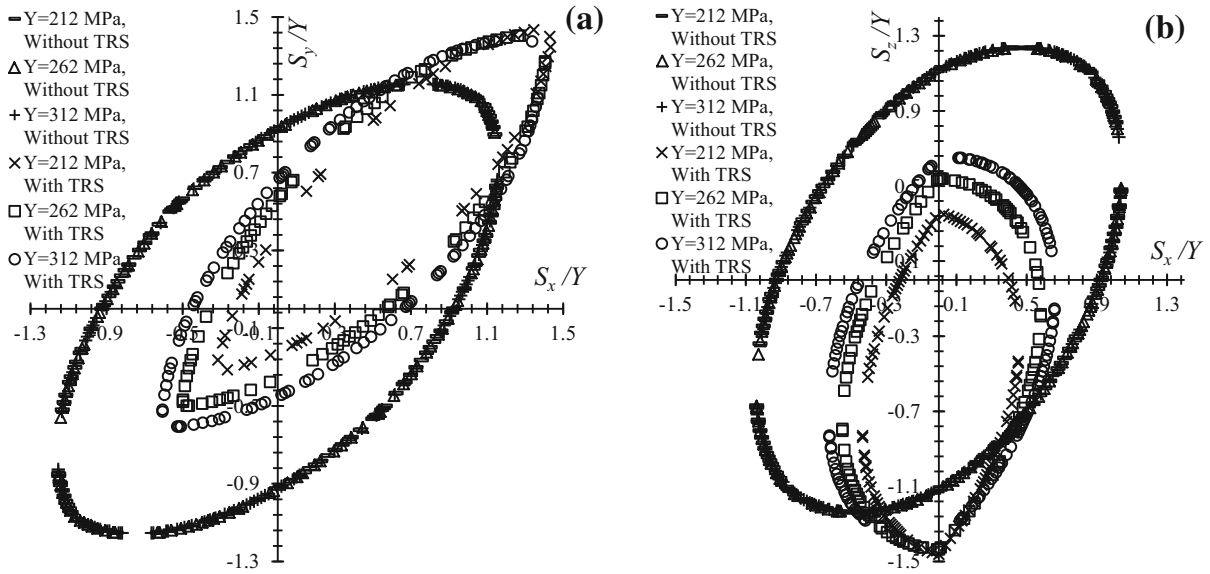


**Fig. 9** Effect of yield strength of Al matrix on the initial yield surfaces in **a** transverse–transverse and **b** longitudinal–transverse stress spaces

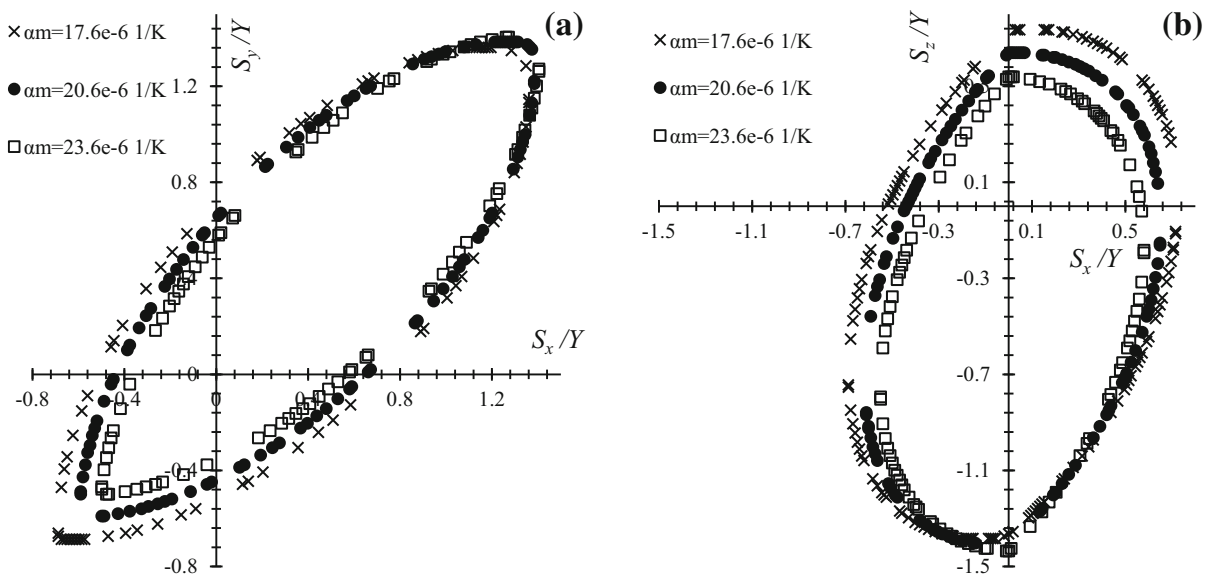


**Fig. 10** Effect of CTE of Al matrix on the initial yield surfaces in **a** transverse–transverse and **b** longitudinal–transverse stress spaces

nanocomposite in uniaxial longitudinal tension decreases as the value of $\alpha_m$ increases.

## 5 Conclusion

The role of TRS on the initial yield envelopes of the CNT-reinforced Al nanocomposites subjected to biaxial loading was investigated by using the SUC micromechanical approach. It was found that the initial yield surfaces were very sensitive to the TRS. Moreover, the results illustrated that with interphase region, the TRS has the highest effect on the yielding behavior of nanocomposites. The size of initial yield surfaces was minimum with considering both the effects of TRS and interphase. Also, the influences of

several important factors such as temperature change, interphase thickness, CNT volume fraction and material properties of Al matrix on the yielding response of CNT/Al nanocomposites were explored. It was found that the size of initial yield surfaces of nanocomposite decreases with increasing the (1) temperature change, (2) interphase thickness, (3) Al matrix elastic modulus and (4) CTE of Al matrix. Furthermore, in the presence of TRS, the size of normalized initial yield surfaces increases as the yield strength of Al matrix increases. It was observed that in the absence of TRS, the yielding behavior of nanocomposites was slightly affected by the variation of CNT volume fraction, while in the presence of TRS, the variation in the value of CNT volume fraction considerably affects the initial yield surfaces of CNT/Al nanocomposites.

## References


Aghdam, M.M., Smith, D.J., Pavier, M.J.: Asymmetric behaviour of fibrous metal matrix composites. Mater. Sci. Technol. **17**, 1153–1157 (2001)

Alfonso, I., Navarro, O., Vargas, J., Beltrán, A., Aguilar, C., González, G., Figueroa, I.A.: FEA evaluation of the $Al_4C_3$ formation effect on the Young's modulus of carbon nanotube reinforced aluminum matrix composites. Compos. Struct. **127**, 420–425 (2015)

Alian, A.R., Kundalwal, S.I., Meguid, S.A.: Interfacial and mechanical properties of epoxy nanocomposites using different multiscale modeling schemes. Compos. Struct. **131**, 545–555 (2015a)

Alian, A.R., Kundalwal, S.I., Meguid, S.A.: Multiscale modeling of carbon nanotube epoxy composites. Polymer **70**, 149–160 (2015b)

Altenpohl, D.G.: Aluminum: technology, applications and environment: a profile of a modern metal aluminum from within, 6th edn. Wiley, Warrendale (1998)

Ansari, R., Hassanzadeh-Aghdam, M.K.: Micromechanics-based viscoelastic analysis of carbon nanotube-reinforced composites subjected to uniaxial and biaxial loading. Compos. Part B **90**, 512–522 (2016a)

Ansari, R., Hassanzadeh-Aghdam, M.K.: Micromechanical investigation of creep-recovery behavior of carbon nanotube-reinforced polymer nanocomposites. Int. J. Mech. Sci. **115–116**, 45–55 (2016b)

Ansari, R., Hassanzadeh-Aghdam, M.K.: Micromechanical characterizing elastic, thermoelastic and viscoelastic properties of functionally graded carbon nanotube reinforced polymer nanocomposites. Meccanica (2016c). doi:10.1007/s11012-016-0512-1

Ansari, R., Hassanzadeh-Aghdam, M.K., Darvizeh, A.: On elastic modulus and biaxial initial yield surface of carbon nanotube-reinforced aluminum nanocomposites. Mech. Mater. **101**, 14–26 (2016)

Aydogdu, M., Arda, M.: Torsional vibration analysis of double walled carbon nanotubes using nonlocal elasticity. Int. J. Mech. Mater. Des. **12**, 71–84 (2016)

Bakshi, S.R., Agarwal, A.: An analysis of the factors affecting strengthening in carbon nanotube reinforced aluminum composites. Carbon **49**, 533–544 (2011)

Bakshi, S.R., Keshri, A.K., Singh, V., Seal, S., Agarwal, A.: Interface in carbon nanotube reinforced aluminum silicon composites: thermodynamic analysis and experimental verification. J. Alloys Compd. **481**, 207–213 (2009)

Baxter, S.C., Robinson, C.T.: Pseudo-percolation: critical volume fractions and mechanical percolation in polymer nanocomposites. Compos. Sci. Technol. **71**, 1273–1279 (2011)

Belytschko, T., Xiao, S.P., Schatz, G.C., Ruoff, R.S.: Atomistic simulations of nanotube fracture. Phys. Rev. B **65**, 235430 (2002)

Cai, J., Li, G., Wang, C., Xie, Z.: Structure of graphene, and mechanical and bonding characteristics of single wall carbon nanotube by linear scaling quantum mechanical method. J. Mater. Sci. Technol. **26**, 614–618 (2010)

Choi, B.K., Yoon, G.H., Lee, S.: Molecular dynamics studies of CNT-reinforced aluminum composites under uniaxial tensile loading. Compos. Part B **91**, 119–125 (2016)

Ci, L., Ryu, Z., Jin-Phillipp, N.Y., Ruhle, M.: Investigation of the interfacial reaction between multi-walled carbon nanotubes and aluminum. Acta Mater. **54**, 5367–5375 (2006)

Demczyk, B.G., Wang, Y.M., Cumings, J., Hetman, M., Han, W., Zettl, A., Ritchie, R.O.: Direct mechanical measurement of the tensile strength and elastic modulus of multiwalled carbon nanotubes. Mater. Sci. Eng., A **334**, 173–178 (2002)

Esawi, A.M.K., Morsi, K., Sayed, A., Taher, M., Lanka, S.: Effect of carbon nanotube (CNT) content on the mechanical properties of CNT-reinforced aluminium composites. Compos. Sci. Technol. **70**, 2237–2241 (2010)

Fisher, F.T., Bradshaw, R.D., Brinson, L.C.: Effects of nanotube waviness on the modulus of nanotube-reinforced polymers. Appl. Phys. Lett. **80**, 4647 (2002)

Han, Y., Elliott, J.: Molecular dynamics simulations of the elastic properties of polymer/carbon nanotube composites. Comput. Mater. Sci. **39**, 315–323 (2007)

He, C., Zhao, N.Q., Shi, C.S., Song, S.Z.: Mechanical properties and microstructures of carbon nanotube-reinforced Al matrix composite fabricated by in situ chemical vapor deposition. J. Alloys Compd. **487**, 258–262 (2009)

Herasati, S., Zhang, L.: A new method for characterizing and modeling the waviness and alignment of carbon nanotubes in composites. Compos. Sci. Technol. **100**, 136–142 (2014)

Joshi, U.A., Sharma, S.C., Harsha, S.P.: Effect of carbon nanotube orientation on the mechanical properties of nanocomposites. Compos. Part B **43**, 2063–2071 (2012)

Junfeng, X., Lijing, X., Meguid, S.A., Siqin, P., Jie, Y., Yu, Z., Ruo, L.: An atomic-level understanding of the strengthening mechanism of aluminum matrix composites reinforced by aligned carbon nanotubes. Comput. Mater. Sci. **128**, 359–372 (2017)

Kashyap, K.T., Koppad, P.G., Puneeth, K.B., Aniruddha Ram, H.R., Mallikarjuna, H.M.: Elastic modulus of multiwalled carbon nanotubes reinforced aluminium matrix

nanocomposite—a theoretical approach. Comput. Mater. Sci. **50**, 2493–2495 (2011)
Kiani, Y.: Free vibration of FG-CNT reinforced composite skew plates. Aerosp. Sci. Technol. **58**, 178–188 (2016)
Kundalwal, S.I., Meguid, S.A.: Micromechanics modelling of the effective thermoelastic response of nano-tailored composites. Eur. J. Mech. A/Solids **53**, 241–253 (2015)
Kundalwal, S.I., Ray, M.C.: Micromechanical analysis of fuzzy fiber reinforced composites. Int. J. Mech. Mater. Des. **7**, 149–166 (2011)
Kundalwal, S.I., Ray, M.C.: Effective properties of a novel composite reinforced with short carbon fibers and radially aligned carbon nanotubes. Mech. Mater. **53**, 47–60 (2012a)
Kundalwal, S.I., Ray, M.C.: Effective properties of a novel continuous fuzzy-fiber reinforced composite using the method of cells and the finite element method. Eur. J. Mech. A/Solids **36**, 191–203 (2012b)
Kundalwal, S.I., Ray, M.C.: Effect of carbon nanotube waviness on the effective thermoelastic properties of a novel continuous fuzzy fiber reinforced composite. Compos. Part B **57**, 199–209 (2014)
Liu, Y.J., Chen, X.L.: Evaluations of the effective material properties of carbon nanotube-based composites using a nanoscale representative volume element. Mech. Mater. **35**, 69–81 (2003)
Liu, Z.Y., Xiao, B.L., Wang, W.G., Ma, Z.Y.: Tensile strength and electrical conductivity of carbon nanotube reinforced aluminum matrix composites fabricated by powder metallurgy combined with friction stir processing. J. Mater. Sci. Technol. **30**, 649–655 (2014)
Long, X., Bai, Y., Algarni, M., Choi, Y., Chen, Q.: Study on the strengthening mechanisms of Cu/CNT nano-composites. Mater. Sci. Eng., A **645**, 347–356 (2015)
Mahmoodi, M.J., Aghdam, M.M., Shakeri, M.: Micromechanical modeling of interface damage of metal matrix composites subjected to off-axis loading. Mater. Des. **31**, 829–836 (2010)
Meguid, S.A., Al Jahwari, F.: Modeling the pullout test of nanoreinforced metallic matrices using molecular dynamics. Acta Mech. **225**, 1267–1275 (2014)
Nafar Dastgerdi, J., Marquis, G., Salimi, M.: The effect of nanotubes waviness on mechanical properties of CNT/SMP composites. Compos. Sci. Technol. **86**, 164–169 (2013)
Ngabonziza, Y., Li, J., Barry, C.F.: Electrical conductivity and mechanical properties of multiwalled carbon nanotube reinforced polypropylene nanocomposites. Acta Mech. **220**, 289–298 (2011)
Nouri, N., Ziaei-Rad, S., Adibi, S., Karimzadeh, F.: Fabrication and mechanical property prediction of carbon nanotube reinforced aluminum nanocomposites. Mater. Des. **34**, 1–14 (2012)
Pal, G., Kumar, S.: Modeling of carbon nanotubes and carbon nanotube–polymer composites. Prog. Aerosp. Sci. **80**, 33–58 (2016)
Pan, Y., Weng, G.J., Meguid, S.A., Bao, W.S., Zhu, Z.H., Hamouda, A.M.S.: Interface effects on the viscoelastic characteristics of carbon nanotube polymer matrix composites. Mech. Mater. **58**, 1–11 (2013)
Pantano, A., Cappello, F.: Numerical model for composite material with polymer matrix reinforced by carbon nanotubes. Meccanica **43**, 263–270 (2008)
Park, J.G., Keum, D.H., Lee, Y.H.: Strengthening mechanisms in carbon nanotube-reinforced aluminum composites. Carbon **95**, 690–698 (2015)
Ray, M.C.: A shear lag model of Piezoelectric composite reinforced with carbon nanotubes-coated Piezoelectric fibers. Int. J. Mech. Mater. Des. **6**, 147–155 (2010)
Seidel, G.D., Lagoudas, D.C.: Micromechanical analysis of the effective elastic properties of carbon nanotube reinforced composites. Mech. Mater. **38**, 884–907 (2006)
Sharma, M., Sharma, V.: Chemical, mechanical, and thermal expansion properties of a carbon nanotube-reinforced aluminum nanocomposite. Int. J. Miner. Metall. Mater. **23**, 222–233 (2016)
Shazed, M.A., Suraya, A.R., Rahmanian, S., Mohd Salleh, M.A.: Effect of fibre coating and geometry on the tensile properties of hybrid carbon nanotube coated carbon fibre reinforced composite. Mater. Des. **54**, 660–669 (2014)
Shindo, Y., Narita, F., Okura, S., Takeda, T., Fu, C.: Electromechanical bending response of PZT/CNT-based polymer laminates subjected to concentrated load. Int. J. Mech. Mater. Des. **10**, 193–197 (2014)
Silvestre, N., Faria, B., Canongia, J.N.: Lopes. Compressive behavior of CNT-reinforced aluminum composites using molecular dynamics. Compos. Sci. Technol. **90**, 16–24 (2014)
Song, H.Y., Zha, X.W.: Influence of nickel coating on the interfacial bonding characteristics of carbon nanotube–aluminum composites. Comput. Mater. Sci. **49**, 899–903 (2010)
Starke Jr., E.A., Staley, J.T.: Application of modern aluminum alloys to aircraft. Prog. Aerosp. Sci. **32**, 131–172 (1996)
Tsai, J.L., Tzeng, S.H., Chiu, Y.T.: Characterizing elastic properties of carbon nanotube/polymer nanocomposites using multi-scale simulation. Compos. Part B **41**, 106–115 (2010)
Wernik, J.M., Meguid, S.A.: Multiscale modeling of the nonlinear response of nano-reinforced polymers. Acta Mech. **217**, 1–16 (2011)
Wernik, J.M., Cornwell-Mott, B.J., Meguid, S.A.: Determination of the interfacial properties of carbon nanotube reinforced polymer composites using atomistic-based continuum model. Int. J. Solids Struct. **49**, 1852–1863 (2012)
Xu, Y., Zhang, D., Cai, J., Yuan, L., Zhang, W.: Effects of multiwalled carbon nanotubes on the electromagnetic absorbing characteristics of composites filled with carbonyl iron particles. J. Mater. Sci. Technol. **28**, 34–40 (2012)
Yakobson, B.I., Brabec, C.J., Bernholc, J.: Nanomechanics of carbon tubes: instabilities beyond linear response. Phys. Rev. Lett. **76**, 2511–2515 (1996)
Zarasvand, K.A., Golestanian, H.: Determination of nonlinear behavior of multi-walled carbon nanotube reinforced polymer: experimental, numerical, and micromechanical. Mater. Des. **109**, 314–323 (2016)
Zhu, X., Zhao, Y.G., Wu, M., Wang, H.Y., Jiang, Q.C.: Fabrication of 2014 aluminum matrix composites reinforced with untreated and carboxyl-functionalized carbon nanotubes. J. Alloys Compd. **674**(2016), 145–152 (2016)